



# A comparative examination of the aerodynamic performance of various seashell-shaped wind turbines

Hossam Hamid<sup>\*</sup>, Rafea Mohamed Abd El Maksoud

Mechanical Power Engineering Department, Faculty of Engineering - Mattaria, Helwan University, Cairo 11718, Egypt

## ARTICLE INFO

### Keywords:

Wind turbine  
Seashell-shaped turbine  
Aerodynamics performance  
CFD

## ABSTRACT

The seashell-shaped wind turbine (spiral wind turbine SWT), a brand-new form of the horizontal axis wind turbine, is intended for metropolitan use. SWTs have the additional advantage of being installed anywhere without considering their surroundings, as they do not need to be located facing the wind direction. The present work introduces various designs of the rotor of the seashell wind turbine to achieve the greatest performance. Two types of turbine spiral profiles (logarithmic and Archimedean) are investigated with changing the turbine opening angle ( $\theta$ ). Utilizing the turbulence model SST  $k-\omega$ , the equations of Reynolds-averaged Navier-Stokes (RANS) are solved and hence the power coefficient ( $C_p$ ) is calculated. A comprehensive comparison of the findings for both configurations indicates that the turbine of the Archimedean spiral profile with  $\theta$  of  $60^\circ$  generates the best performance. The seashell wind turbine with the Archimedean profile at a  $\theta$  of  $60^\circ$  has a maximum  $C_p = 0.266825$  at  $\lambda = 2.5$ . The seashell wind turbine with the Archimedean profile has the best performance than traditional Archimedes wind turbines which were studied previously by other researchers. The maximum percentage increase in the  $C_p$  of the seashell turbine with the Archimedean profile compared to the conventional Archimedes turbine equals 14.52%.

## 1. Introduction

Energy is the issue that developing nations face the most difficulties in the procedure of sustainable advancement. Researchers are working to create a new energy source to reduce our reliance on fossil fuels due to the exponential population growth. Furthermore, despite having a negative impact on the climate, a thriving human civilization depends on fossil fuel energy, and its use is growing quickly. Global warming, greenhouse gas pollution, accelerated climate change, and ozone layer depletion are all caused by current energy sources, primarily fossil fuels. Renewable energy is one of the most convenient and environmentally friendly options available, depending on the natural resources of each nation. Green technology adoption and production improvement are currently significant issues. Wind energy is an alternative to generating electric power with no pollution [1,2].

Wind energy has recently proven to be an important resource and an environmentally friendly method compared to other energy sources. Alternative energy sources to coal, oil, natural gas, and nuclear power plants include wind energy. It is regarded as one of the greenest sources of energy in the world, which is not affected by the sunrise or the sunset the same as solar energy. The technology is fairly advanced, there is no air or water pollution created, and while the turbine has been installed and the operating cost is almost zero, this is in terms of the environmental impact. In general, the use of wind turbines to produce electricity has spread quickly. The

<sup>\*</sup> Corresponding author.

E-mail addresses: [eng.hossamsaed@gmail.com](mailto:eng.hossamsaed@gmail.com), [hossam.saeed@m-eng.helwan.edu.eg](mailto:hossam.saeed@m-eng.helwan.edu.eg) (H. Hamid).

**Nomenclature [units]**

$P$	Turbine power [W]
$T$	Total torque [N.m]
$F_L$	Lift force [N]
$F_D$	Drag force [N]
$F_N$	Normal force [N]
$F_T$	Tangential force [N]
$AR$	Aspect ratio [–]
$P$	Static pressure [Pa]
$C_T$	Turbine torque coefficient [–]
$C_P$	Turbine power coefficient [–]
$Z$	Number of turbine blades [–]
$N$	Turbine rotational speed [rpm]
$y^+$	Non-dimensional wall distance
$Re$	Reynolds number [–]
$U_\infty$	Wind velocity [m/s]
$k$	Turbulence kinetic energy [ $m^2/s^2$ ]
$S$	Spiral pitch [mm]
$r$	Turbine radius [mm]

**Greek symbols**

$\rho$	Air density [ $kg/m^3$ ]
$\Omega$	Specific dissipation rate [–]
$\theta$	Turbine opening angle [°]
$\lambda$	Tip-speed ratio [–]
$\Omega_o$	Turbine angular speed [rad/s]
$\mu$	Air dynamic viscosity [ $kg/m.s$ ]

**Abbreviations**

SWT	Spiral wind turbine
ASWT	Archimedean spiral wind turbine
HAWT	Horizontal-axis wind turbine
VAWT	Vertical-axis wind turbine
RANS	Reynolds-Averaged Navier-Stokes
CFD	Computational Fluid dynamics
MRF	Moving Reference Frame
TSR	Tip Speed Ratio
PS	Pressure Surface
SS	Suction Surface

**Subscripts**

$s$	Static
-----	--------

**Superscripts**

–	Mean
^	Estimator

areas wherever such techniques are to be applied and used, particularly in urban areas, are still quite a few. There are many different methods used by wind turbines; the turbine being considered in this work combines VAWTs and HAWTs.

A contemporary form of wind turbines is the seashell-shaped wind turbine, also called the spiral wind turbine (SWT). The SWT is an innovative kind of horizontal-axis wind turbine that was built utilizing the spiral theory. SWT comprises three conic blades that wrap around one another in a set spiral pattern to complete a cycle. It produces a conical-shaped rotor as a result. In contrast to typical VAWTs or HAWTs, which either use drag or lift forces to obtain power from the wind, the SWT utilizes together the lift and drag forces [3]. A schematic illustration of the forces that aerodynamically act on the blade of the SWT is shown in Fig. 1. The SWT's use of low-wind kinetic energy and compact design are two of its distinctive features. The SWT is appropriate for urban areas with low wind velocity because its cut-in wind speed is lower than other wind turbines [4,5,6,7]. A small capacity SWT suitable for domestic or urban environments is shown in Fig. 2.

In some situations, such as those close to buildings, the advantages of the SWT are more obvious because it works at low wind velocities. The wind's direction constantly varies within the metropolitan area. SWT is guided automatically to face the wind path due

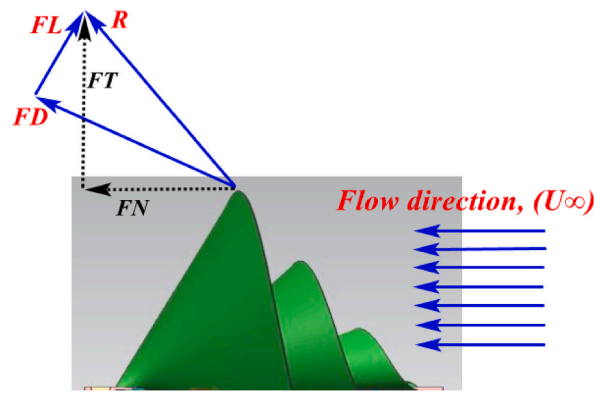


Fig. 1. Schematic illustration of the aerodynamic forces affecting on the rotor of the SWT.

to its passive control. However, the SWT system can adapt quickly to turbulent flow and remains effective at higher wind speeds and even in hurricane conditions [4,5,6,7].

Furthermore, the SWT is capable of compensating for wind direction variation. As a result, due to the benefits of the unique design of turbine blades, no electronic yawing equipment is required. Therefore, even when the wind direction changes rapidly, the SWT remains as a controllable yaw-type wind turbine. Additionally, the turbine produces less noise than all other wind turbines that is because of the turbine’s relatively slow rotating speed [4,5]. Thus, these relatively lower noise levels make the SWT an optimal choice for installation near residential areas where concerns about noise are elevated.

There have been certain previous studies illustrated in the literature review that attempts to measure and improve the performance of the SWTs. Experimental and numerical examinations of the SWT on a small scale were conducted by Kim et al. [5] using the PIV measurements and the CFD way, respectively. The outcomes showed that at  $\lambda = 2$ , the turbine generates its maximum power and has a maximum  $C_p = 0.25$ . The potential and the best performance characteristics of the SWT were investigated by Timmer and Toet [8] using laser practice. The results showed that 12% was the maximum efficiency that could be measured.

Ebrahimi and Ghassemi [9] applied the solver ANSYS-CFX in their numerical research to evaluate the performance of the SWTs. The findings confirmed that, for various wind speeds, the turbine demonstrates the highest  $C_p$  equals 0.26 at  $TSR = 2.5$ . Safdari et al. [10] used both numerical and PIV practices to assess the SWT features. The flow behaviors around an SWT as well as the flow wake behind its blades were both investigated by the authors. Findings showed that the highest turbine power coefficient was attained at a  $TSR$  equal to 2.5 and equal to 0.25. Ozeh et al. [11] measured the SWT performance in an empirical test. The results showed that the turbine’s optimum  $\lambda$  equal to 1.48 at wind velocity equals 4 m/s.

Jang et al. [12] numerically investigated the SWT, and the experimental outcomes supported the numerical conclusions. According to the results, it can be seen that the turbine’s peak  $C_p$  is equal to 0.293 at a  $TSR$  of roughly 2.19. The aerodynamic performance of the

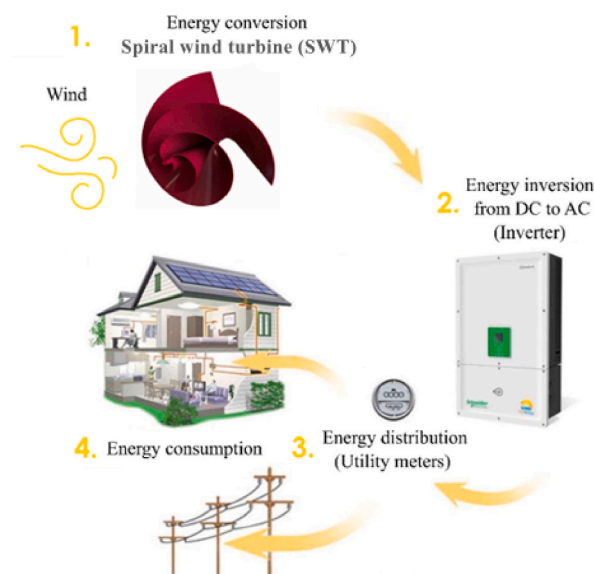


Fig. 2. A layout of a small-capacity spiral wind turbine (SWT).

SWT was evaluated numerically and presented by Patil [13]. The data presented showed that these turbines were perfect for usage in metropolitan regions due to their physical characteristics against flow disturbance.

Additionally, Mustafa and Jaleel [14] conducted an experimental evaluation of the outputs of the propeller wind turbine and the ASWT. The results showed that the ASWT performs better than a wind turbine with a propeller. ASWT characteristics and the overall turbine performance were also analyzed by Ostia et al. [15], who also compared the ASWT's performance with that of the Savonius wind turbine. The evaluation's findings demonstrated that the performance of the ASWTs is more excellent than the Savonius turbines at similar wind velocities.

Experimental evaluations on a 0.5 kW model of the ASWT were done by Ji et al. [16]. The used design demonstrated that the highest  $C_p$  as a function of the TSR is comparable to the propeller-type turbine's ideal efficiency. The ASWT aerodynamic characteristics were the main topic of an experimental study by Chaudhary et al. [17]. Findings confirmed that the turbine's cut-in wind velocity was approximately 2.5 m/s. Additionally, Chaudhary et al. [17] demonstrated a unique yaw system that could direct the turbine's rotor to the wind's direction without requiring electronic devices, thus showing a new way to enhance the performance of the turbine.

The ASWT performance was evaluated numerically based on the CFD strategy and presented through Nepal et al. [18]. The computational outcomes of this investigation indicated that the highest  $C_p$  equal to 0.25 was obtained at a TSR equal to 1.5. A computational and experimental assessment to evaluate the performance of the turbine was performed by Nawar et al. [6]. It offered a thorough assessment of the turbine's complete performance throughout various terminal speed ratios and wind speeds. The turbine's performance was examined concerning the impacts of altering the blade angle. The outcomes demonstrated that the variable blade angle model performed better than the fixed blade one.

Also, Using the ANSYS-CFX program, the influence of aspect ratio on the aerodynamic performance of small-scale ASWT was numerically evaluated for wind velocities ranging from 5 to 12 m/s [19] Labib et al. The findings showed that the turbine has its maximum  $C_p$  of 0.249 at TSR equal to 1.413 at AR close to unity. Experimental trials and simulation techniques have been used to examine how the ASWT's performance is impacted by changing the blade angle from 50° to 65° [20] Labib et al. The outcomes showed that the turbine with an angle equal to 50° has the best performance and that the maximum  $C_p$  is 0.22 at TSR equal to 1.72. Additionally, at a tip speed ratio equal to 2, linking the ASWT with a concentrator boosted a maximum  $C_p$  by 33.48% in comparison to the bare turbine [7]. The optimal concentrator arrangement was discovered at an angle of the concentrator equal to 20°, a position equal to 0.1 of the turbine diameters, a tip clearance equal to 0.05 of the diameter of the turbine, and a concentrator length equal to 0.6 of the diameter of the turbine. Table 1 summarizes the most important previous investigations on spiral wind turbine design alterations and their effects on the turbine's performance.

A review of previous studies may conclude that no clear information on the aerodynamic performance of the seashell-shaped wind

**Table 1**

Summary of the previous studies related to the spiral wind turbine (SWT).

Modification	Description	Outcome
Wind direction "Ji et al. (2016) [4]"	The effect of wind direction was examined experimentally using the 2D PIV method for measurement planes from 0° to 15°.	The results indicated that the trajectory of tip vortices varies significantly in the front-side plane compared to that of a lee-side plane at an angle of attack of 10°.
Aerofoil blade "Rao et al. (2018) [16]"	An aerofoil of NACA 6409 profile was introduced to the blade of an Archimedean-spiral wind turbine by CREO and ANSYS FLUENT software packages.	The Archimedes aerofoil wind turbine with NACA 6409 substantially increased the torque by 15% as compared to the Archimedes wind turbine at moderate wind speed.
Pitch and blade angle "Nepal et al. (2019) [17]"	The effect of some geometrical parameters such as pitch and opening angle on the performance of an Archimedean-spiral type wind turbine was investigated at wind speeds ranging from 3.5 m/s to 12 m/s through CFD simulations.	It was suggested that a pitch of 1.5 times the radius and an opening angle of 60° gives the highest power coefficient of the Archimedean spiral-type wind turbine.
Yawing mechanism "Chaudhary 2016 [18]"	A passive-type yawing mechanism is introduced to a small-scale horizontal-axis wind turbine adopting Archimedean-spiral rotor blades to turn the rotor against the wind direction without the need for any electronic devices.	The Archimedean-spiral wind turbine is proved to produce higher torque than other types of wind turbines at low wind speeds and the passive-type yawing mechanism employed in this work resulted in reducing the cost of such a turbine.
Variable-angle rotor "Nawar et al. (2020) [6]"	Both experimental and numerical evaluations were launched on two variants of Archimedean-spiral type wind turbine; one with a fixed-angle rotor and the other with a variable-angle rotor.	The variable-angle design showed some excellence on the fixed-angle design at moderate tip-speed ratios since the variable-angle rotor exhibited a 14.7% increase in output power compared to the fixed-angle rotor.
Aspect ratio "Labib et al. (2020) [19]"	The effect of aspect ratio on the aerodynamic performance of a small-scale Archimedes spiral wind turbine was assessed numerically for wind speeds ranging from 5 to 12 m/s using ANSYS-CFX 19 software.	The results highlighted that a maximum power coefficient of 0.249 was achieved at a tip-speed ratio of 1.413 for aspect ratio with front-side elongation equal to unity.
Blade Angle "Labib et al. (2021) [20]"	Computational simulations and experimental trials were carried out to investigate the effect of blade angle on the performance of a scaled-down Archimedean-spiral wind turbine. The blade angle was changed from 50° to 65°.	The maximum value of the power coefficient was recorded as 0.22 at $\lambda = 1.72$ when the blade angle of the scaled-down Archimedean-spiral type wind turbine is 50°.
Concentrator "Refaie et al. (2021) [7]"	Qualitative and quantitative assessments of the aerodynamic characteristics of a concentrator-augmented Archimedean-spiral wind turbine were carried out using a campaign of 3D numerical simulations.	In comparison to the bare Archimedean-spiral wind turbine, the concentrator-augmented Archimedean-spiral wind turbine showed an enhancement in the power of about 33.48% for concentrator inclination angle of 20°, tip-clearance of 0.1r, and concentrator length of 1.2r.

turbine related to the spiral profile of the turbine or the turbine opening angle is currently available. The seashell-shaped wind turbine is distinguished from other turbines in that its operating speed is low compared to vertical (Savonious or Darrieus) or conventional horizontal axis wind turbines. Also, these turbines do not need to direct the wind to them, as they are self-propelled and face the wind from any direction. These turbines are also characterized by the ability to produce energy at low wind speeds with a low noise ratio, which qualifies them to operate in urban areas.

The present work aims to analyze the turbine’s performance through a numerical study using ANSYS fluent software and identify the aerodynamic turbine characteristics and the most important parameters that affect the turbine’s performance. The present research also seeks to introduce the best configuration of the turbine with the highest turbine performance with the possibility of increasing the operating range of the turbine. As a result of the lack of information and research gap for this type of wind turbine, the effect of the type of spiral on the performance of the turbine is studied. Also, the effect of changing the opening angle of the turbine on its performance is studied for both types of the spiral. Due to the lack of information on this particular type of wind turbine and a small research space. So the current work is believed to be an extraordinary item in its field for comprehending the complex movement across such turbines and getting the perfect structure for the highest performance of the turbine.

**2. Model description**

A spiral wind turbine (SWT) typically comprises three blades wrapped around one shaft to form the turbine. Each blade forms a rotor with a triangular base and is symmetrically arranged around its shaft. SWT has the potential to reverse the direction of the approaching wind to capture the available kinetic energy. Fig. 3 Defines the parameters used in the SWT design. For instance, the spiral pitch (S) denotes the axial distance measured whenever the spiral profile performs one cycle. The turbine radius (r) signifies the radial distance between the blade tip at the exit and the axis of rotation, and the turbine opening angle (θ), indicates the angle between the axis of rotation and the blade tip at the outlet.

In the presented work, the SWT performance is studied with more than one principle, such as the logarithmic and Archimedes principle, with the study of changing the opening angle on the performance. Fig. 4 displays different models of the spiral profile logarithmic spiral and Archimedean spiral. Fig. 4(a) shows the spiral wind turbine with a logarithmic profile, while Fig. 4(b) shows the turbine with an Archimedean profile. The logarithmic spiral can be distinguished from the Archimedean spiral by the fact that the distances between the turnings of a logarithmic spiral increase in geometric progression. In contrast, in an Archimedean spiral, these distances are constant.

The Archimedean spiral has the following equation in the polar coordinate system:

$$r = a + b * t \tag{1}$$

Whereas the polar equation of the logarithmic spiral is given by,

$$r = a * e^{bst} \tag{2a}$$

Where a and b are arbitrary constants, t is the angle of rotation of the spiral, and r is the length of the radius from the center or beginning of the spiral. For each spiral turbine, the opening angle was changed from 40° to 90° with a step of 10°. Fig. 5 illustrates the

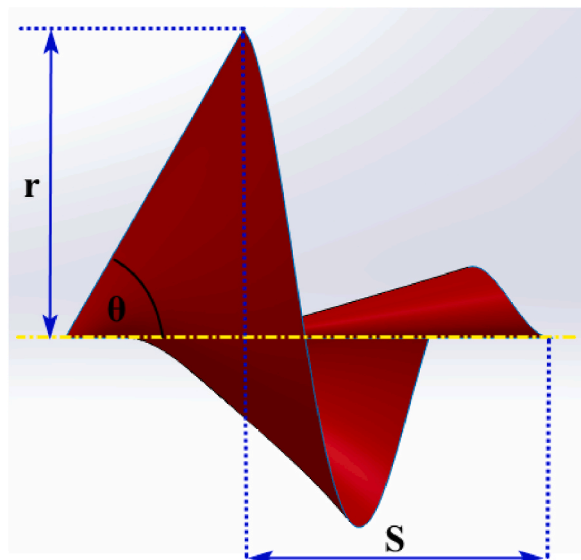


Fig. 3. Definition of the parameters used in the SWT design.

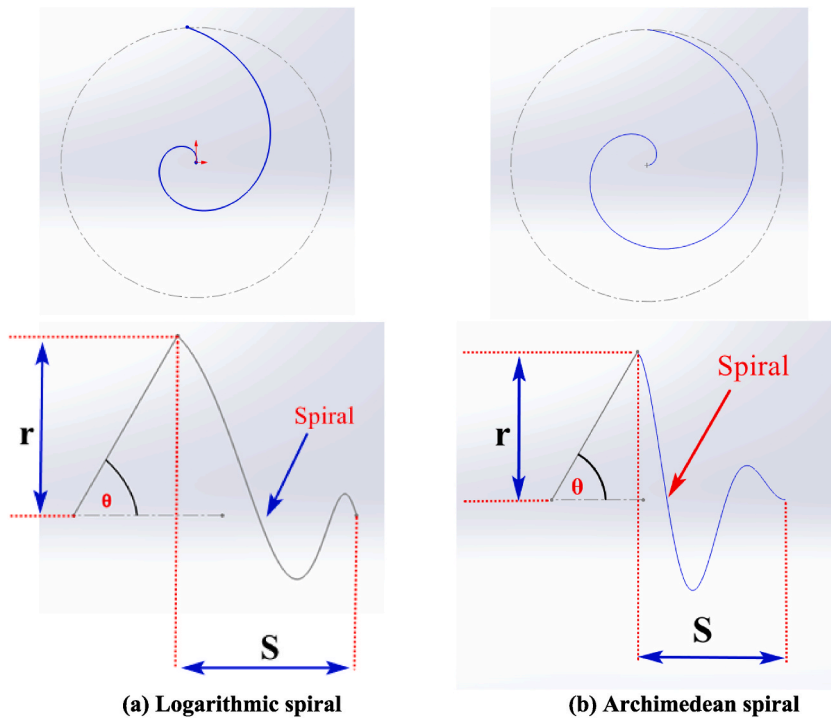


Fig. 4. Different models of the spiral profile of the seashell-shaped wind turbines.

various configuration of the seashell-shaped wind turbine based on the opening angle for logarithmic and Archimedean spiral. As Fig. 5 (a) presents different shapes of the spiral turbine with a logarithmic profile depending on the change of opening angle ( $\theta = 40^\circ$  to  $\theta = 90^\circ$ ), while Fig. 5(b) presents different models of the turbine with Archimedean profile according to the value of the opening angle ( $\theta = 40^\circ$  to  $\theta = 90^\circ$ ).

The aerodynamic interaction between the spiral blades and the approaching wind flow determines how much power the SWT produces. The CP is a measurement of the amount of energy that an SWT extracts from the wind flow. The relation between both the velocity of the wind ( $U_\infty$ ) and the rotor blade tip speed ( $\Omega r$ ) is another crucial idea in determining how effectively an SWT will operate, and this relationship is named the tip speed ratio ( $\lambda$ ). The important elements that affect an SWT's output of power are briefly

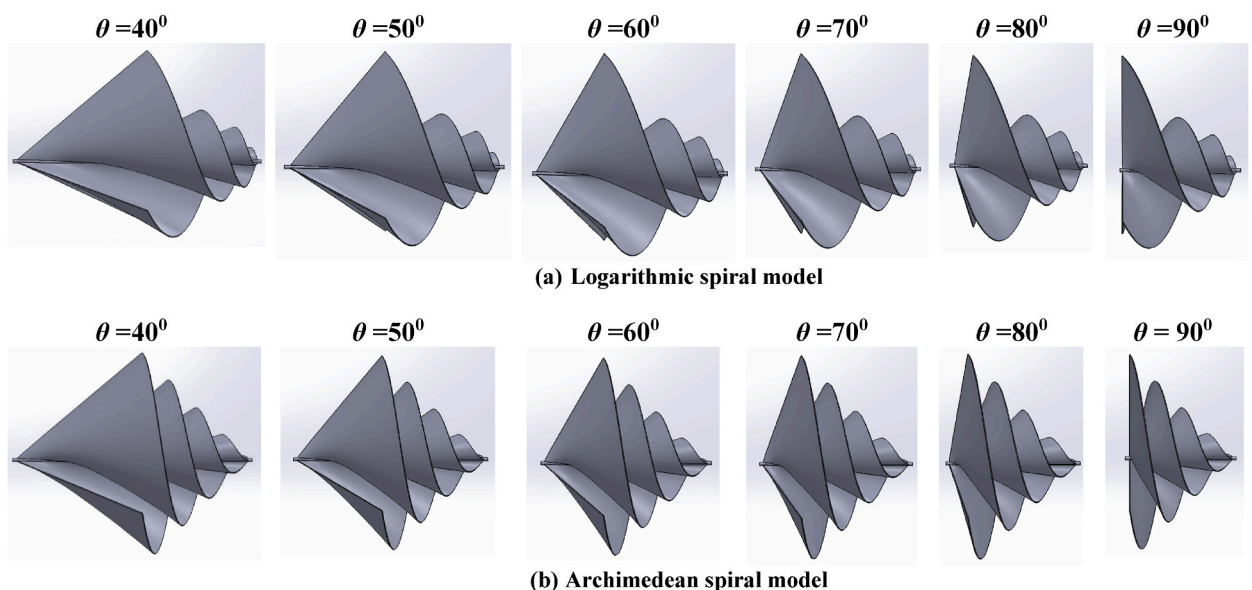
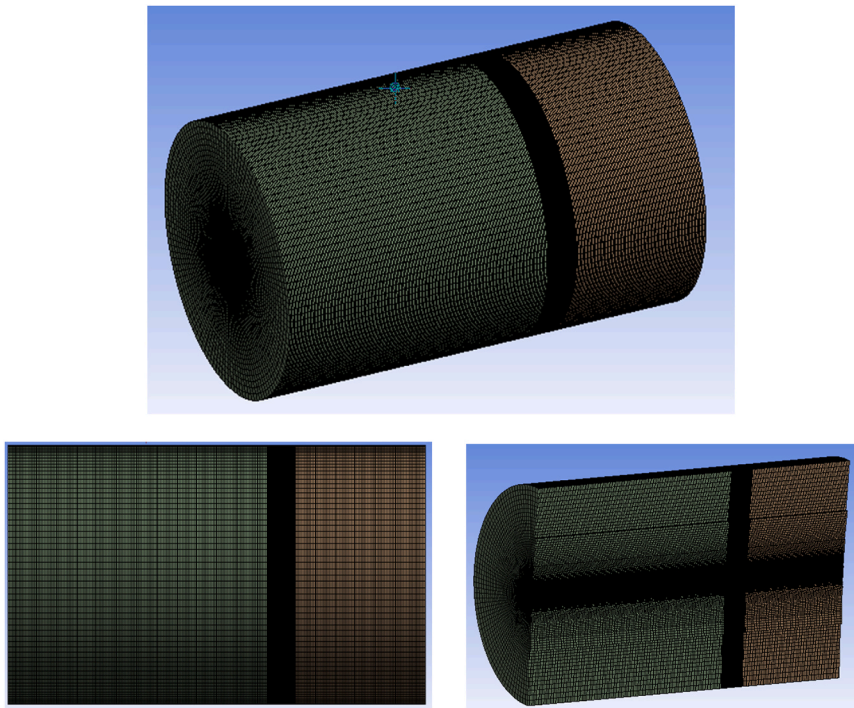
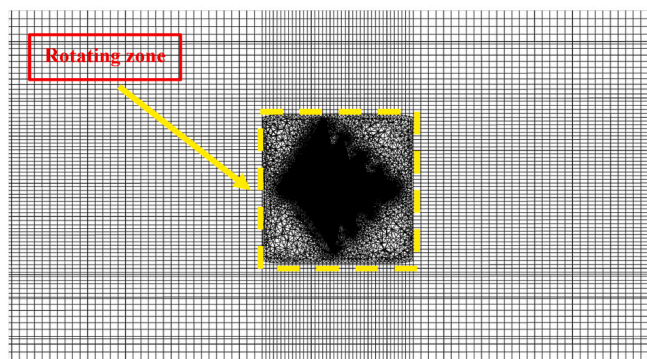
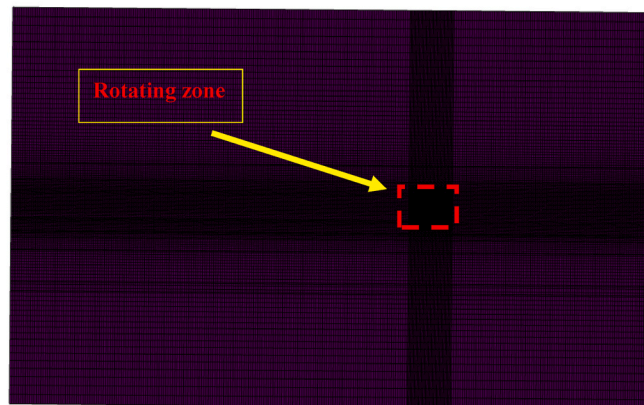


Fig. 5. Different designs of the seashell-shaped wind turbine based on the opening angle, (a) Logarithmic spiral (b) Archimedean spiral.



(a) 3D view.



(b) Rotating domain.

(caption on next page)

Fig. 6. The computational grid: (a) 3D view of the whole domain, (b) rotating domain.

covered in this section.

Equation (2b) defines  $\lambda$ :

$$\lambda = \frac{\Omega_o r}{U_\infty} \tag{2b}$$

Where  $\Omega_o$  defines the turbine angular speed,  $U_\infty$  defines the velocity of the wind, and  $r$  expresses the SWT's radius.

The SWT coefficient of performance ( $C_p$ ) may be denoted as illustrated in equation (3).

$$C_p = \frac{T \Omega_o}{0.5 \rho A U_\infty^3} \tag{3}$$

wherever  $T$  states the turbine torque,  $\rho$  defines the air density, and  $A$  ( $A = \pi r^2$ ) is the turbine projected area, under normal conditions  $\rho$  may be equal to  $1.225 \text{ kg/m}^3$ .

### 3. Numerical simulation

To demonstrate the airflow across the wind turbine, common numerical simulation techniques such as the Reynolds Average Navier Stokes (RANS) through the MRF methodology are taken. Such a method takes the benefit of describing the revolution of the turbine blade without needing the computational mesh to be moved because all the equations that govern the fluid flow are set up in the rotational reference frame. The governing equations in the commercial ANSYS-FLUENT coding package are used for solving the steady-state RANS equations. Since the flow is configured to be incompressible as long as the Mach number is less than 0.3, the only factor affecting the continuity equation is the flow velocity expression, as displayed in Eq (4). Where the term that describes the flow pressure is presented in the momentum equation, as displayed in Eq. (5). A direct methodology is adopted to attain the effects of the pressure, after which discrete amounts are then used in the momentum equation (Eq (5)) and continuity (Eq (4)) equation and solved simultaneously. The 3D incompressible flow will be governed and controlled through the next equations [21]:

Mass conservation equation:

$$\frac{\partial \bar{U}_i}{\partial x_i} = 0 \tag{4}$$

Momentum equation

$$\frac{\partial \bar{U}_i}{\partial t} + \frac{\partial \bar{U}_i \bar{U}_j}{\partial x_j} = -\frac{1}{\rho} \frac{\partial \bar{p}}{\partial x_i} + \nu \frac{\partial^2 \bar{U}_i}{\partial x_i \partial x_j} - \frac{\partial \bar{u}_i \bar{u}_j}{\partial x_j} \tag{5}$$

where the Cartesian axis is represented by the numbers  $i = 1, 2, \text{ and } 3$ ; and  $\bar{U}_i, x_i$  are the component of the mean velocity and the Cartesian length respectively. The expression  $(\bar{u}_i \bar{u}_j)$  defines the Reynolds stress, that symbolizes the stresses brought on by fluctuations.  $\rho, p,$  and  $\nu$  represents the fluid density, fluid pressure, and kinematic viscosity respectively. The velocity vectors are specified by  $U_i$  and  $U_j$  in the  $i$  and  $j$  directions. Equations (4) and (5) are time-averaged governing forms and were used to produce the solutions of RANS for the steady-state approach this is when the term of the time could be disregarded.

Firstly, A CAD program is used to model the geometry of the SWT, which is later introduced to the Design Modeler software in order to establish an appropriate domain for the computational study. The presented numerical domain is well-defined as the cylindrical form. The rotating domain is located 20 times the radius of the turbine rotor from the domain outlet and located 10 times the radius of the turbine rotor from the intake of the domain. Additionally, the stationary domain's diameter is 10, as recommended from the

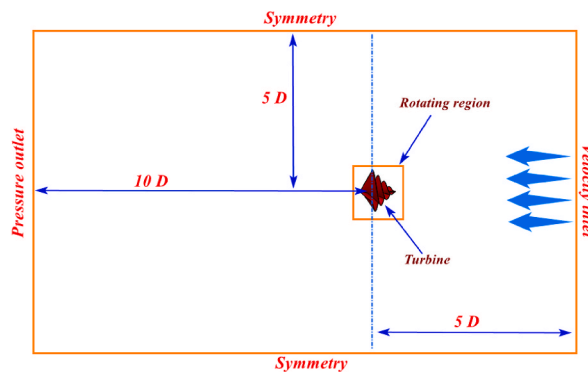


Fig. 7. Illustration of the computational domain as well as the solution boundary conditions.

previous studies [6,22], see Fig. 7. The ANSYS Meshing tool is used to generate the mesh. It is decided to use a hybrid mesh made up of 6,131,302 hexahedral/tetrahedral cells. There are 15 prismatic layers along with a growth rate of 1.2 for all the boundaries of the wall. The height of the first layer close to the spiral blade surface is fixed at 0.003 mm in order to get  $y^+$  less than 1 under all operating circumstances. The mesh configurations that comprise both fixed and revolving domains are shown in Fig. 6. Whereas, Fig. 6(a) presents a 3D view of the mesh that includes the entire domain, while Fig. 6(b) presents a close-up and enlarged view of the mesh of the rotating domain. The moving domain's grid elements are positioned in the interior of the stationary domain. In light of this, they are divided using the technique of the MRF. The equations of the MRF are used to resolve the flow in each rotating cell region.

#### 4. Fundamentals of the CFD solvers

The ANSYS Fluent program was employed in this work for 3D CFD simulation. The selected grid is introduced using ANSYS Fluent, and the solver setup is complete. The fluid characteristics and the specified turbulent model are determined during the setup process. CFD Fluent has several turbulence models that are used to anticipate flow separation, one of which is the Shear Stress Transport SST  $k-\omega$  turbulence model. It is made up of a two-equation model. Turbulent model SST  $k-\omega$  takes benefits of together  $k-\omega$  and  $k-\epsilon$  turbulent models, wherever  $k$  is the turbulent kinetic energy,  $\epsilon$  is the rate of dissipation of the turbulent kinetic energy,  $\omega$  and is the specific rate of dissipation [23,24].

Using the turbulent model SST  $k-\omega$ , the turbulent flow surrounding the turbine's rotor has been modeled as an incompressible and steady-state flow. The turbulence model SST  $k-\omega$  was used within the proposed numerical works that is because it expects flow pattern and the separation of the flow with a precise simulation approach after that delivers acceptable results at near-wall boundary layers. Moreover, various research [6,20,21] have already endorsed turbulent model SST  $k-\omega$  for similar purposes.

The equation of mass conservation and that of Navier-Stokes are two of the most important governing equations. For the continuity and momentum equations, Reynolds average form is employed, and turbulent model SST  $k-\omega$  is then applied to resolve them. As these equations are configured in the rotational reference frame with the turbine, the simulations can describe the rotation of the blade without necessitating the grid to rotate. To solve the partial differential equations in the form of an algebraic equation, the Finite Volume Method (FVM) is utilized. In ANSYS, these massive algebraic equations are seamlessly reversed by an iterative approach.

The equations of the turbulent model SST  $k-\omega$  (Eq. (6) and Eq. (7)) can be expressed in the following manner [6,21,23]:

$$\frac{\partial}{\partial t}(\rho k) + \frac{\partial}{\partial x_i}(\rho k u_i) = \frac{\partial}{\partial x_j} \left[ \Gamma_k \frac{\partial k}{\partial x_j} \right] + G_k - Y_k + S_k \tag{6}$$

$$\frac{\partial}{\partial t}(\rho \omega) + \frac{\partial}{\partial x_i}(\rho \omega u_i) = \frac{\partial}{\partial x_j} \left[ \Gamma_\omega \frac{\partial \omega}{\partial x_j} \right] + G_\omega - Y_\omega + S_\omega \tag{7}$$

where  $G_k$  defines the turbulent kinetic energy emergence based on a mean velocity gradient. The generation of  $\omega$  is defined by  $G_\omega$ .  $Y_k$  and  $Y_\omega$  signify the dissipative of  $k$  and  $\omega$  owing to turbulent, respectively, while  $D_\omega$  indicates the term of the cross-diffusion. Also,  $S_k$  and  $S_\omega$  are describing the terms of the user-defined sources. Eq. (8) represent the effective diffusivity ( $\Gamma_\omega$ ) of  $\omega$  and Eq. (9) represent the effective diffusivity ( $\Gamma_k$ ) of  $k$ , and are derived using the following formulas [6,21,23]:

$$\Gamma_k = \mu + \frac{\mu_t}{\sigma_k} \tag{8}$$

$$\Gamma_\omega = \mu + \frac{\mu_t}{\sigma_\omega} \tag{9}$$

where  $\mu_t$  denoting the turbulent viscosity, and  $\sigma_\omega$  and  $\sigma_k$  expressing the turbulence Prandtl numbers for  $\omega$  and  $k$ , respectively. As illustrated in Fig. 7, the boundary conditions for this analysis are at the domain entry the flow velocity is set to 8 m/s, and the pressure is set to atmospheric pressure at the outlet of the domain. The turbine blades are subjected to the No-Slip condition. After initializing the system, equations are solved. Table 2 includes a summary of the grid settings and solver boundary conditions.

The non-dimensional wall distance ( $y^+$ ) was reduced to less than one to accurately predict the flow patterns near the wall layer (the sub-layer and the buffer zone) for the turbulence model SST  $k-\omega$ , as well as offer a sufficient prediction of the turbine's aerodynamic

**Table 2**  
Characteristics of the grid and the solution boundary conditions.

Parameter	Description
Mesh/Nature	Hexahedral/Tetrahedral
Elements	6,131,302
Fluid	Air
Turbulence model	SST $k-\omega$
Inlet	Velocity (8 m/s)
Outlet	Pressure
Turbine rotor	Wall
Farfield	Symmetry
Maximum residual	$10^{-6}$

performance [25,26]. As shown in Table 3, various discretization techniques were used during the simulation. The pressure-velocity coupling was carried out using the coupling methodology. For the continuity, moment, and the turbulence equations, the solution's highest residual values were  $10^{-6}$ .

## 5. Results and discussion

### 5.1. Mesh independence study

To make sure that the numerical outcomes are independence on the size of the cell or independent on the resolution of the mesh, a mesh independence study is a crucial procedure. This step is carried out to diminish or lessen the impact of the cell number or the size of the cells on the computational outcomes. So, in the presented work, the computational grid was evaluated and tested through the mesh-independent study in order to ensure the quality of the presented grid. The cell number ranged from 710,500 cells to 6,131,302 cells. This was performed with the constancy of the first layer thickness, the number of prismatic layers, and a growth rate of the blade and shaft surface, to maintain non-dimensional wall distance  $y^+ < 1$  at the same  $\lambda$ . Fig. 8 depicts the influence of cell number on  $C_p$  at a  $\lambda$  of 2. It is noted that the  $C_p$  stays constant with an inaccuracy of less than 1% at a mesh size of around 3 million. For the best solution quality, a cell number of 6,131,302 was used for the computational analysis presented in this work, where CFD results are independent of the cell number in the selected computational domain.

### 5.2. Validation of CFD results

To guarantee the quality and accuracy of the presented numerical model, the computational data of the SWT simulation have been compared and validated with those from the previously published studies [5,6]. The SWT performance is described in the current study in the term of a dimensionless turbine power coefficient " $(C_p)$ ". A comparison of the simulated and practical SWT outcomes at various  $\lambda$ -values are shown in Fig. 9. The similarity in trend between the computational findings and the experimental data is underlined. As shown in Fig. 9, the introduced numerical data suggest a maximum  $C_p$  of 0.2668 at  $\lambda = 2.5$ , whereas the previous works [5] show a maximum  $C_p$  of 0.26 at  $\lambda = 2.25$ . In terms of  $C_p$ , there is good consistency between previously published data [5,6] and current data. As a result, the validation is deemed successful. It is clear that the presented results agree well with the previously published results, as the maximum error rate between the results is less than 5% and the output curves have the same style and trend. The validation process has goals through which the quality and accuracy of the numerical model presented are confirmed. Accordingly, the present CFD model has been greatly admitted as a computational tool for the performance of the spiral turbine. After that, the performance of the seashell-shaped wind turbine is investigated when changing the spiral profile (logarithmic, Archimedean) along with changing the opening angle value.

### 5.3. Effect of varying the value of the opening angle ( $\theta$ ) on the performance of the seashell-shaped wind turbine with a logarithmic spiral profile

The seashell-shaped wind turbine performance that has a logarithmic spiral profile is investigated numerically with changing the opening angle  $\theta$ . Fig. 10 shows the relationship between the torque coefficient  $C_T$  of a logarithmic spiral turbine with the turbine TSR at several turbine opening angles. It is clear from this figure that the  $C_T$  decreases with an increasing TSR. Also, it is noticed from this figure that turbines with small  $\theta$  have a high  $C_T$ , and that is only at a low TSR of less than 1. On the contrary, turbines with large  $\theta$  have the best  $C_T$  with an increase in the TSR. According to Fig. 10, it is concluded that at TSR greater than 0.75 the turbine with  $\theta$  of  $90^\circ$  achieves the highest  $C_T$  rather than all other modules. Also, it is observed that the turbine with a  $\theta$  of  $40^\circ$  has the lowest  $C_T$ , see Fig. 10.

Fig. 11 shows the relationship between the power coefficient  $C_p$  and the tip speed ratio. It is noticeable that the logarithmic spiral seashell-shaped wind turbine performance improves together with the increase in the value of the  $\theta$ , as illustrated in Fig. 11. It was found that the turbine with a  $\theta$  of  $90^\circ$  achieves the best performance and the best operating range over the other shapes. Also, the turbine with  $\theta = 40^\circ$  has the worst performance and the least operating range. Whereas The turbine with  $\theta$  equal to  $90^\circ$  exhibits a maximum  $C_p$  of 0.20858 at a value of TSR equal to 1.75.

Figs. 12–14 depict the velocity contours, static pressure contours, and pressure coefficient contours of the seashell-shaped wind turbine with a logarithmic spiral profile in the rear region at  $\lambda$  of 1.75 and at a velocity of the flow equal to 8 m/s, respectively. For example, in Fig. 12, it was observed that there are areas with low velocity in the foreground at the beginning of the turbine blades. This region decreased with increasing the opening angle. In contrast, at  $\theta$  greater than  $70^\circ$  (Fig. 12(d)), a zone with high velocity (marked

**Table 3**  
Solver setting.

Pressure-velocity coupling	Coupled
Gradient	Least squares cell-based
Pressure	Second-order
Momentum	Second -order upwind
Turbulent kinetic energy ( $k$ )	Second -order upwind
Specific dissipation rate ( $\omega$ )	Second-order upwind

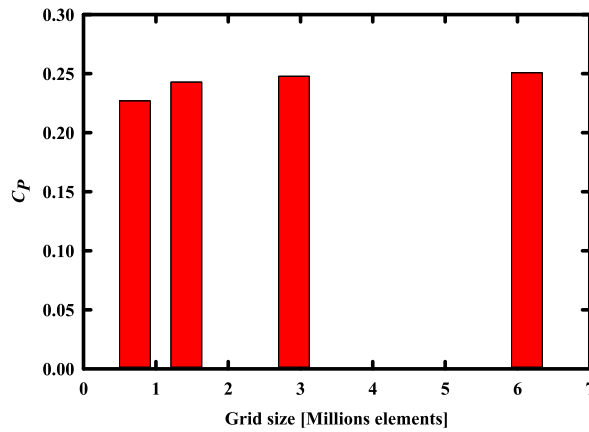


Fig. 8. Grid independence study.

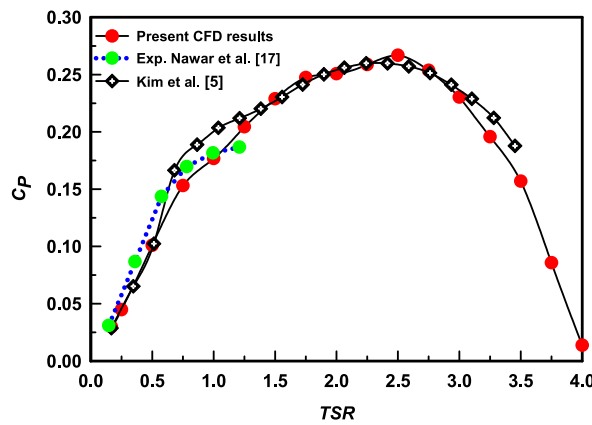


Fig. 9. Comparison of the presented numerical results to previous results [5,6].

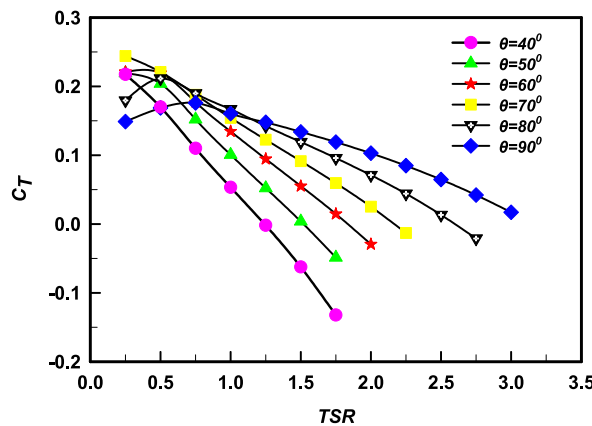


Fig. 10. Comparison of the torque coefficient  $C_T$  of a seashell-shaped wind turbine having a logarithmic spiral profile with different opening angles  $\theta$ .

with a red dashed circle) was created at the front blades. This zone increased with increasing the  $\theta$ . Also, this region is the main reason for increasing the  $C_p$ .

Furthermore, it was mentioned that there was a wake zone behind the turbine at  $\theta$  larger than  $70^\circ$  and that the size of this zone grew as the opening angle rose, see Fig. 12(d). The zone of high velocity in front of the turbine and the wake zone behind it combine to raise the turbine's coefficient of performance ( $C_p$ ). As shown in Fig. 13, a pressure difference is generated across the turbine rotor due to the

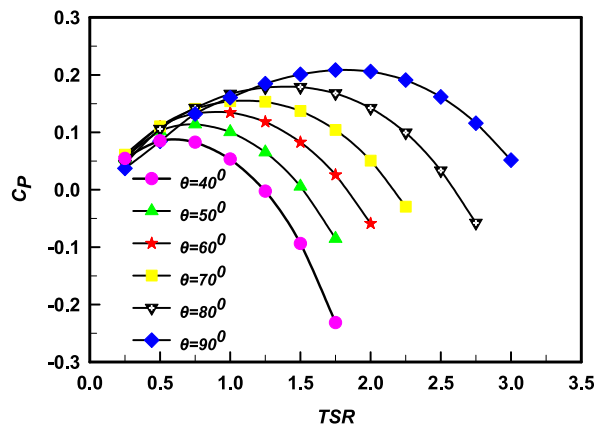


Fig. 11. Comparison of the power coefficient  $C_p$  of a seashell-shaped wind turbine having a logarithmic spiral profile with different opening angles  $\theta$ .

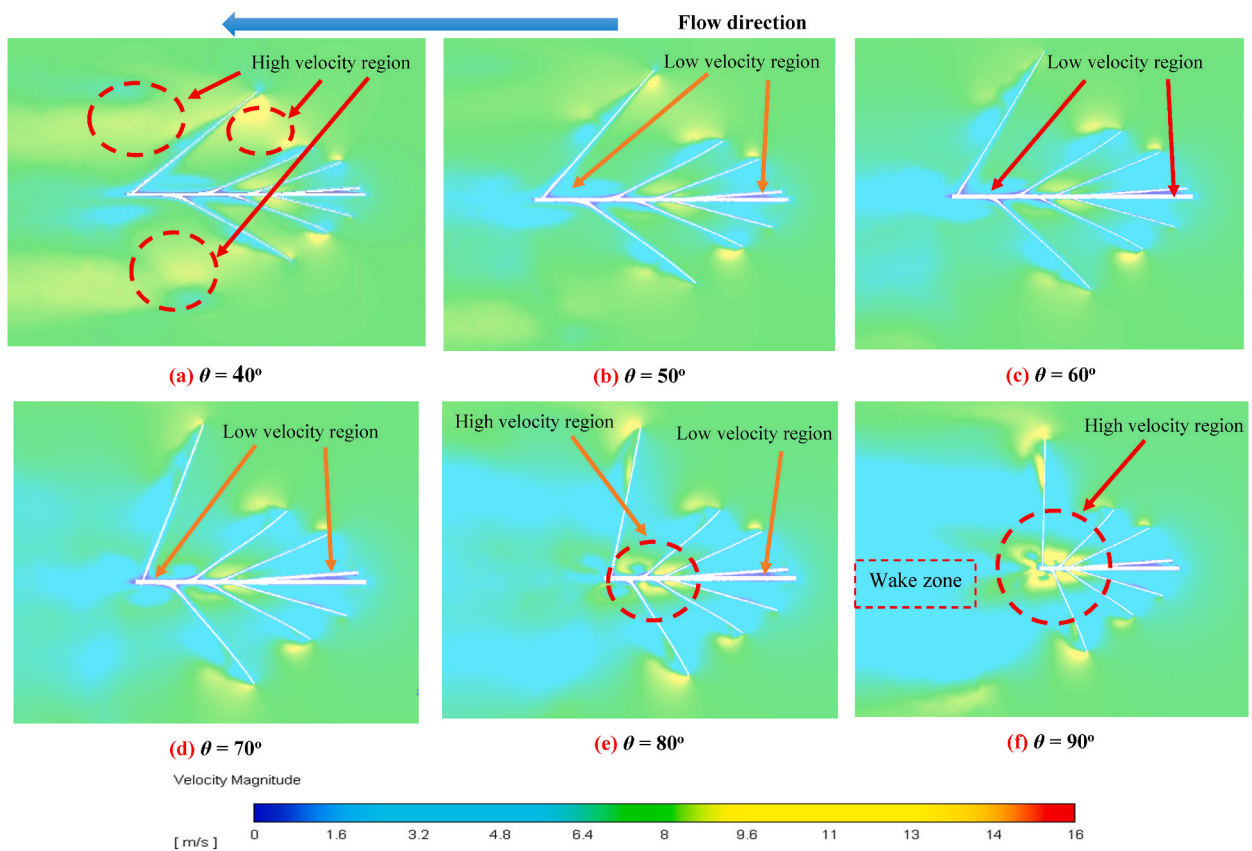


Fig. 12. Velocity contours of seashell-shaped wind turbine having a logarithmic spiral profile at different opening angles ( $\theta$ ) at  $\lambda$  of 1.75.

fluid movement through the turbine rotor and the air momentum. As there is a high-pressure area (marked with a blue dashed circle) created before the turbine and a low-pressure area formed after the turbine. It is also noted that this pressure difference increases with the increase in the opening angle value, see Fig. 13(f). Also, the higher this pressure ratio, the higher the  $C_p$  of the turbine. So, the maximum  $C_p$  is for a turbine with  $\theta$  of  $90^\circ$ .

On the other hand, as shown in Figs. 13 and 14, at  $\theta$  lower than  $70^\circ$  see Figs. 13(d) and Fig. 14(d), a high-pressure region was formed behind the turbine rather than the low-pressure zone, and this leads to reducing the  $C_p$ . But for the turbine with an opening angle ( $\theta$ ) higher than  $70^\circ$ , there was a region of low-pressure created after the rotor of the turbine, this region together with the high-

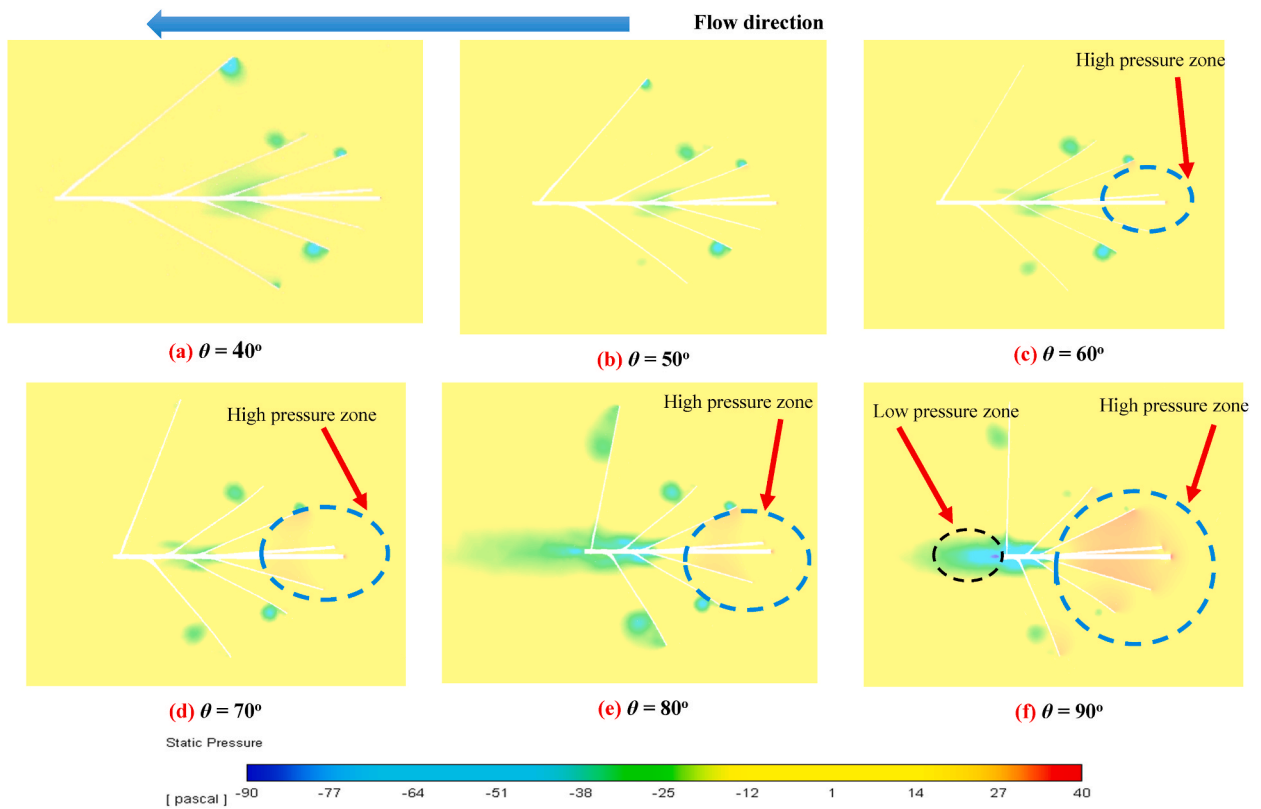


Fig. 13. Pressure contours of seashell-shaped wind turbine having a logarithmic spiral profile at different opening angles ( $\theta$ ) at  $\lambda$  of 1.75.

pressure zone upstream of the turbine, describes why the turbine with a  $90^\circ$  opening angle has the best performance, see Figs. 13(f) and Fig. 14(f).

Also, the contours of the pressure coefficient illustrated in Fig. 14 approves that the turbine at an angle  $\theta$  of  $90^\circ$  achieves the best performance and the maximum  $C_p$ , as there is a very low-pressure zone (marked with a red dashed circle) formed after the turbine rather than all the rest models of the logarithmic spiral turbine (see Fig. 14(f)). The flow fields around the turbine rotor illuminate closely the features of the flow at the turbine. Furthermore, it enables assessing and adjusting the performance of the turbine, which has an important effect on advancing turbine energy production.

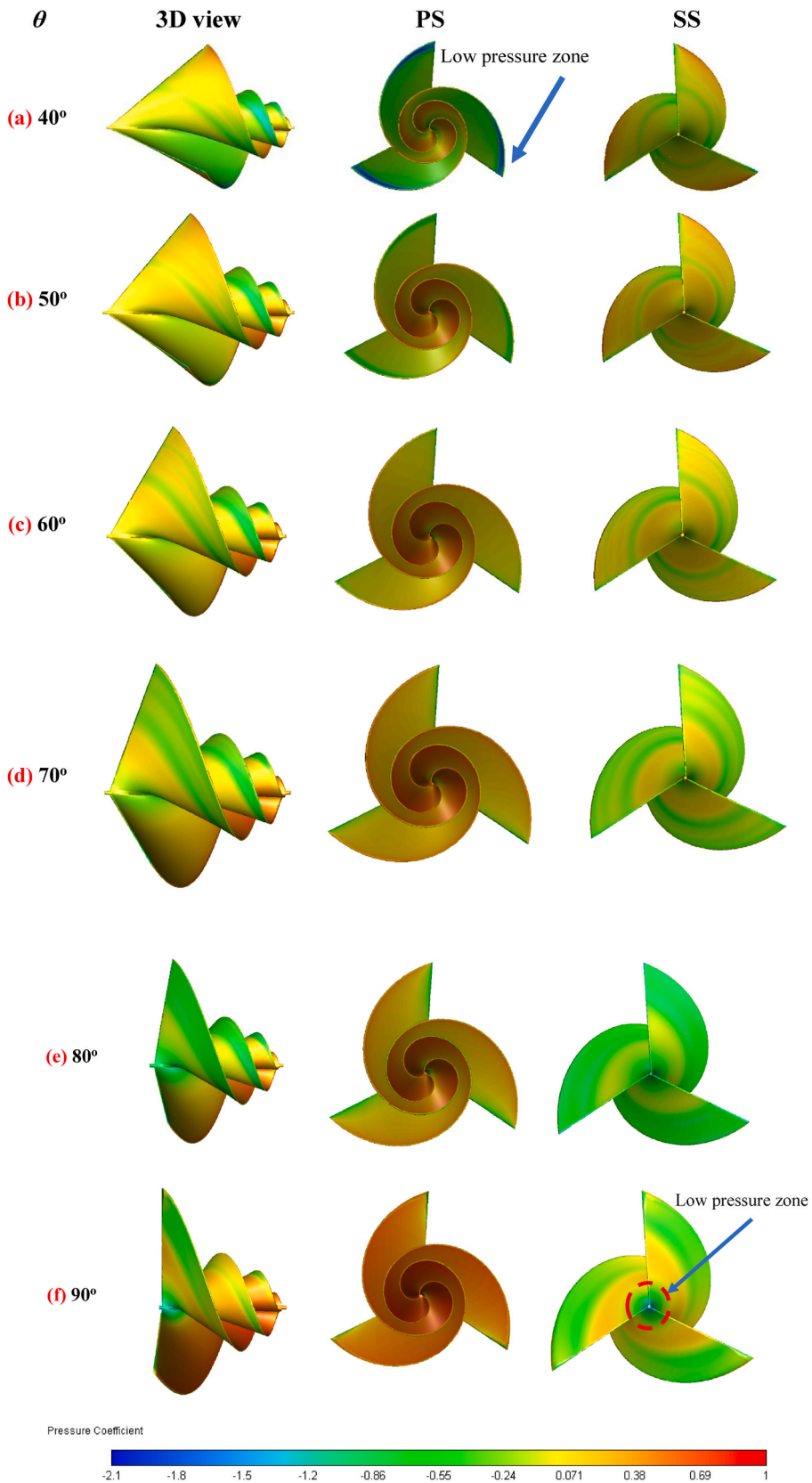
5.4. Effect of varying the value of the opening angle ( $\theta$ ) on the performance of the seashell-shaped wind turbine with an archimedean spiral profile

Fig. 15 shows the relationship between the torque coefficient ( $C_T$ ) of a seashell-shaped Archimedean spiral turbine with the turbine TSR at different turbine opening angles  $\theta$ . It is clear from this fig. that the  $C_T$  decreases with an increasing TSR. Also, it is indicated from this fig. that turbines with small  $\theta$  have a high  $C_T$ , and that is only at a low TSR of less than 2. According to Fig. 15, the maximum  $C_T$  reached 0.27757 and was achieved for a turbine with  $\theta = 40^\circ$  at a TSR of 0.25. On the contrary, turbines with large  $\theta$  have the best  $C_T$  with an increase in the TSR. It's observed that the turbine with a  $\theta$  of  $60^\circ$  has a high  $C_T$  of 0.126 at TSR = 2, see Fig. 15.

The non-dimensional turbine power coefficient ( $C_p$ ) is considered one of the most important external SWT factors. Fig. 16 presents an assessment of the results of the seashell-shaped wind turbine (Archimedean spiral profile) at various opening angles ( $\theta$ ). As shown in Fig. 16, the variability of the  $C_p$  has been recognized for the entire operating range of typical TSR values. It can be concluded from Fig. 16 that the seashell-shaped wind turbine of the Archimedean spiral profile with various  $\theta$  has two different operating ranges (TSR < 2, TSR > 2). At values of TSR lower than 2, the turbine with  $\theta$  equal to  $50^\circ$  has the best performance rather to all other shapes. The highest  $C_p$  was achieved for the turbine with  $\theta$  equal to  $50^\circ$  at TSR = 2 and equals 0.25432. Also, the turbine  $C_p$  decreased with increasing the  $\theta$  during this range (TSR < 2) as illustrated in Fig. 16.

On the other hand, at values of TSR > 2, the  $C_p$  values increased along with increasing the  $C_p$  from  $40^\circ$  to  $70^\circ$ . But at values of  $\theta$  greater than  $70^\circ$ , with increasing the angle value ( $80^\circ$ ,  $90^\circ$ ) the performance is decreased. The maximum  $C_p$  equals 0.2683 at TSR = 2.5 for the turbine with a  $60^\circ$  opening angle. But at values of TSR greater than 2.5, the turbine with  $\theta$  of  $70^\circ$  has the best performance and best operating range than all the shapes. The turbine with  $\theta$  equal to  $70^\circ$  exhibits a maximum  $C_p$  of 0.2588 at a TSR of 2.75.

The velocity contours, static pressure contours, and pressure coefficient contours of the seashell-shaped wind turbine with an Archimedean spiral profile are represented in Fig. 17, Fig. 18, and Fig. 19, respectively. The contours are observed at  $\lambda$  of 2 and a wind



(caption on next page)

Fig. 14. Pressure coefficient contours of seashell-shaped wind turbine having a logarithmic spiral profile at different opening angles ( $\theta$ ) at  $\lambda$  of 1.75.

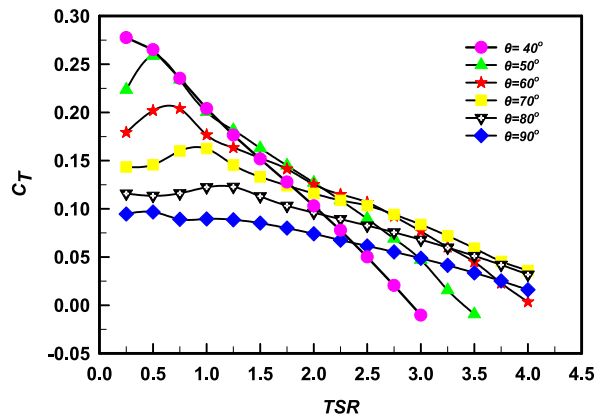


Fig. 15. Comparison of the torque coefficient  $C_T$  of a seashell-shaped wind turbine with different opening angles having an Archimedean spiral profile.

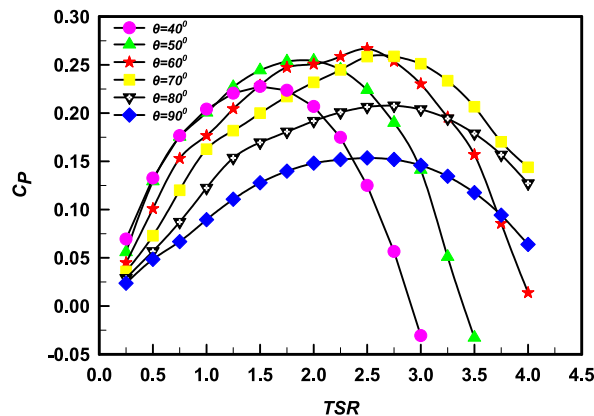


Fig. 16. Comparison of the power coefficient  $C_P$  of a seashell-shaped wind turbine with different opening angles having an Archimedean spiral profile.

velocity equal to 8 m/s. As described in Fig. 17, it can be detected that there is a zone with high velocity at the rear turbine blades, which is marked with a red dashed circle, and this region increased with increasing the  $\theta$ . But at  $\theta$  greater than  $70^\circ$ , this zone declined. On the other hand, at  $\theta$  greater than  $70^\circ$ , a zone with low velocity was founded at the front blades, see Fig. 17(d). This zone increased with increasing the opening angle. This region is considered to be the main reason for decreasing the  $C_p$ . It is noted that there is a wake zone behind the turbine at values of  $\theta$  greater than  $70^\circ$ , and this region increased with increasing the  $\theta$ . This wake zone behind the turbine, together with the low-velocity zone in front of the turbine, results in reducing the turbine  $C_p$ .

According to Fig. 18, High and low-pressure regions were created upstream and downstream of the turbine blades due to the flow momentum. This enhances the pressure difference over the turbine rotor that sequentially raises the turbine torque coefficient ( $C_T$ ) and the power coefficient ( $C_P$ ). As shown in Fig. 18, it was observed that the high-pressure region (marked with a red dashed circle) increased with increasing the  $\theta$ . On the other side, it was found that at  $\theta$  greater than  $60^\circ$  see Fig. 18(c), a high-pressure zone was created behind the turbine rather than a low-pressure zone, leading to decreasing the  $C_p$ .

On the other hand, for the turbine with  $\theta$  equal to  $60^\circ$ , a low-pressure zone was created downstream of the turbine as shown in Fig. 18(c). This region and the high-pressure zone upstream of the turbine rotor explain why the turbine with a  $60^\circ$  opening angle achieves the best performance. Also, the pressure coefficient contours presented in Fig. 19 confirm that the turbine with  $\theta$  equals  $60^\circ$  achieves the best performance see Fig. 19(c). As there is a very low-pressure zone (marked with a black dashed circle) created after the turbine rather than all the rest models (see Fig. 19(c)). Both the velocity and pressure contours nearby the turbine rotor clarify closely the characteristics of the flow at the turbine. Additionally, it permits evaluating and adapting the performance of the turbine which has an important influence on advancing energy production.

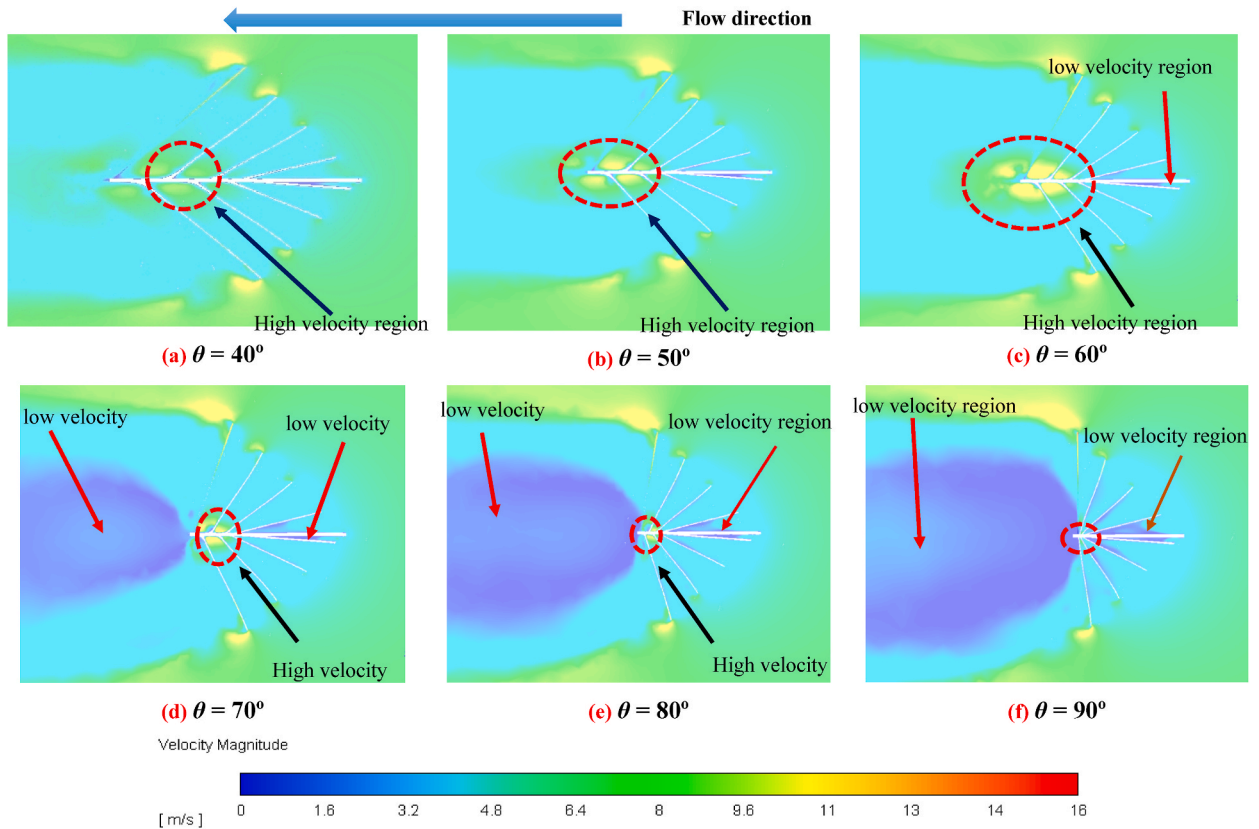


Fig. 17. Velocity contours of a seashell-shaped wind turbine having an Archimedean spiral profile at different opening angles ( $\theta$ ) at  $\lambda$  of 2.

5.5. Comparison of the maximum power coefficient ( $\max C_p$ ) and the average torque coefficient ( $C_{T \text{ average}}$ ) for a seashell-shaped wind turbine having a logarithmic spiral profile and archimedean spiral profile at various opening angles ( $\theta$ )

In order to determine and confirm the performance of the best turbine configuration, the average torque coefficient  $C_{T \text{ Average}}$  and the maximum  $C_p$  were calculated for all configurations presented in this work. Fig. 20 shows a comparison of the  $C_{T \text{ Average}}$  of a seashell-shaped wind turbine having a logarithmic spiral profile at several opening angles ( $\theta$ ). It was found that the lowest value of the  $C_{T \text{ Average}}$  is about 0.05066 for the turbine with a  $\theta$  of 40. It is noted from this fig. that the turbine with an angle of 70° achieves the maximum  $C_{T \text{ Average}}$ , which is equal to 0.1215. The turbine with  $\theta$  of 90° also achieves a large  $C_{T \text{ Average}}$  and equals 0.114. Fig. 21 presents a comparison between the maximum  $C_p$  of the logarithmic spiral turbine at different values of the turbine opening angles. From Fig. 21, it is clear that the maximum  $C_p$  of the turbine with  $\theta$  of 90° is greater than the maximum  $C_p$  of the other configurations and is equal to 0.20858, and this is at a TSR equal to 1.75.

Fig. 22 depicts the  $C_{T \text{ Average}}$  of a seashell-shaped wind turbine with an Archimedean spiral profile at various  $\theta$ . This fig. shows that the turbine with  $\theta$  of 40° obtains the highest  $C_{T \text{ Average}}$ , which is equivalent to 0.13993. The turbine with a  $\theta$  of 90° has the lowest  $C_{T \text{ Average}}$ , which is 0.0654. While Fig. 23 demonstrates a comparison between the maximum  $C_p$  of the Archimedes spiral turbine at various  $\theta$ . According to Fig. 23, the maximum  $C_p$  of the turbine with  $\theta$  of 60° is more than the maximum  $C_p$  of the other configurations and equal to 0.2683 at a TSR equal to 2.5.

The seashell-shaped wind turbine looks very promising, unlike other traditional spiral wind turbines. Fig. 24 presents a comparison between the performance of the seashell-shaped wind turbine having an Archimedean spiral profile and the traditional Archimedes turbine that was studied previously [6]. According to Fig. 24, it is concluded that the proposed study shows a new turbine with better performance and a better operating range than the turbine presented in the previous studies [6]. The turbine presented during this study achieves a maximum  $C_p$  of 0.2683 at a TSR value equal to 2.5. While for the previously studied turbine [6], the maximum  $C_p$  is achieved at a TSR equal to 2 and equal to 0.233. This is an indication that the turbine presented during this study has better aerodynamic performance than the traditional turbines that were previously studied and presented.

The maximum  $C_p$  of the seashell-shaped Archimedes spiral wind turbine is achieved at a TSR of 2.5 and greater than the maximum  $C_p$  of the conventional one achieved at a TSR of 2. At a TSR of 2.5, it was found that the maximum percentage increase in the  $C_p$  of the provided turbine was equal to 32.5% compared to the conventional turbine at the same TSR. Also, it was found that the range of operation of these turbines is better than the traditional ones, see Fig. 24. The  $C_{T \text{ Average}}$  of the provided turbine is also greater than the

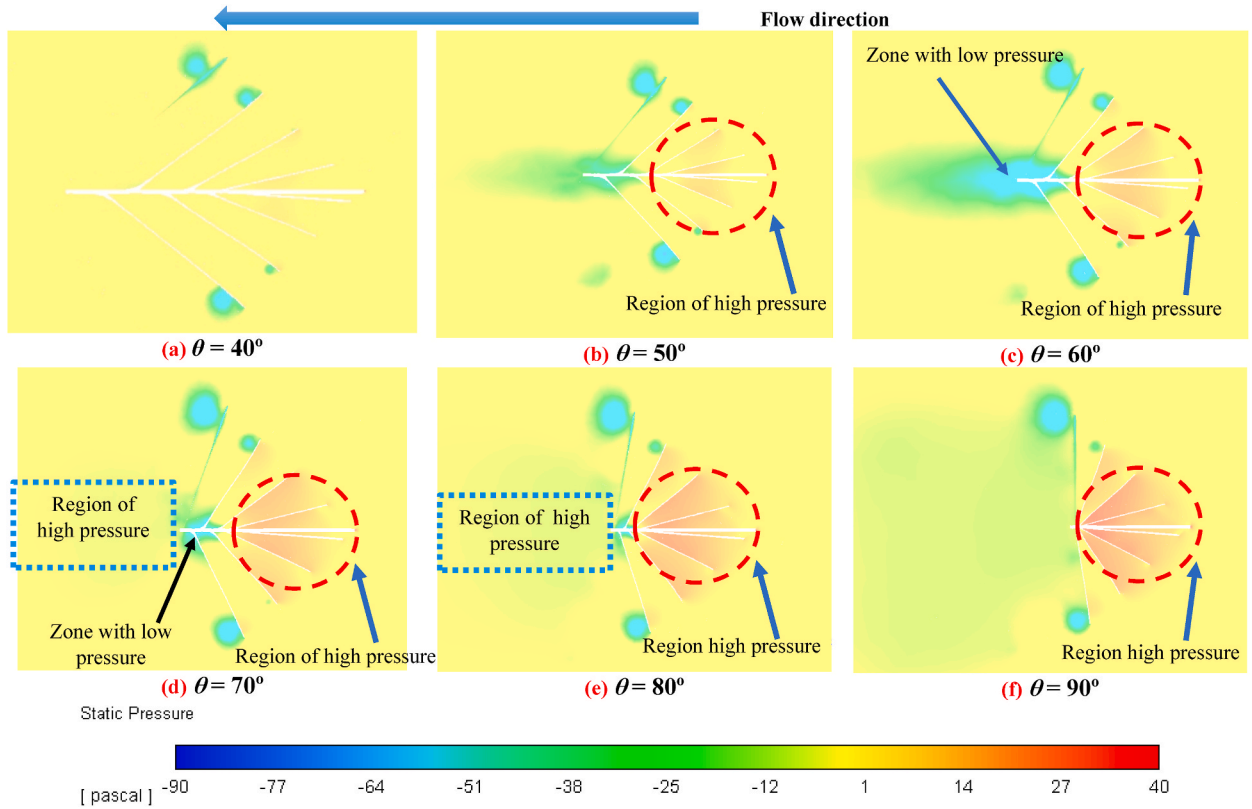


Fig. 18. Pressure contours of a seashell-shaped wind turbine having an Archimedean spiral profile at different opening angles ( $\theta$ ) at  $\lambda$  of 2.

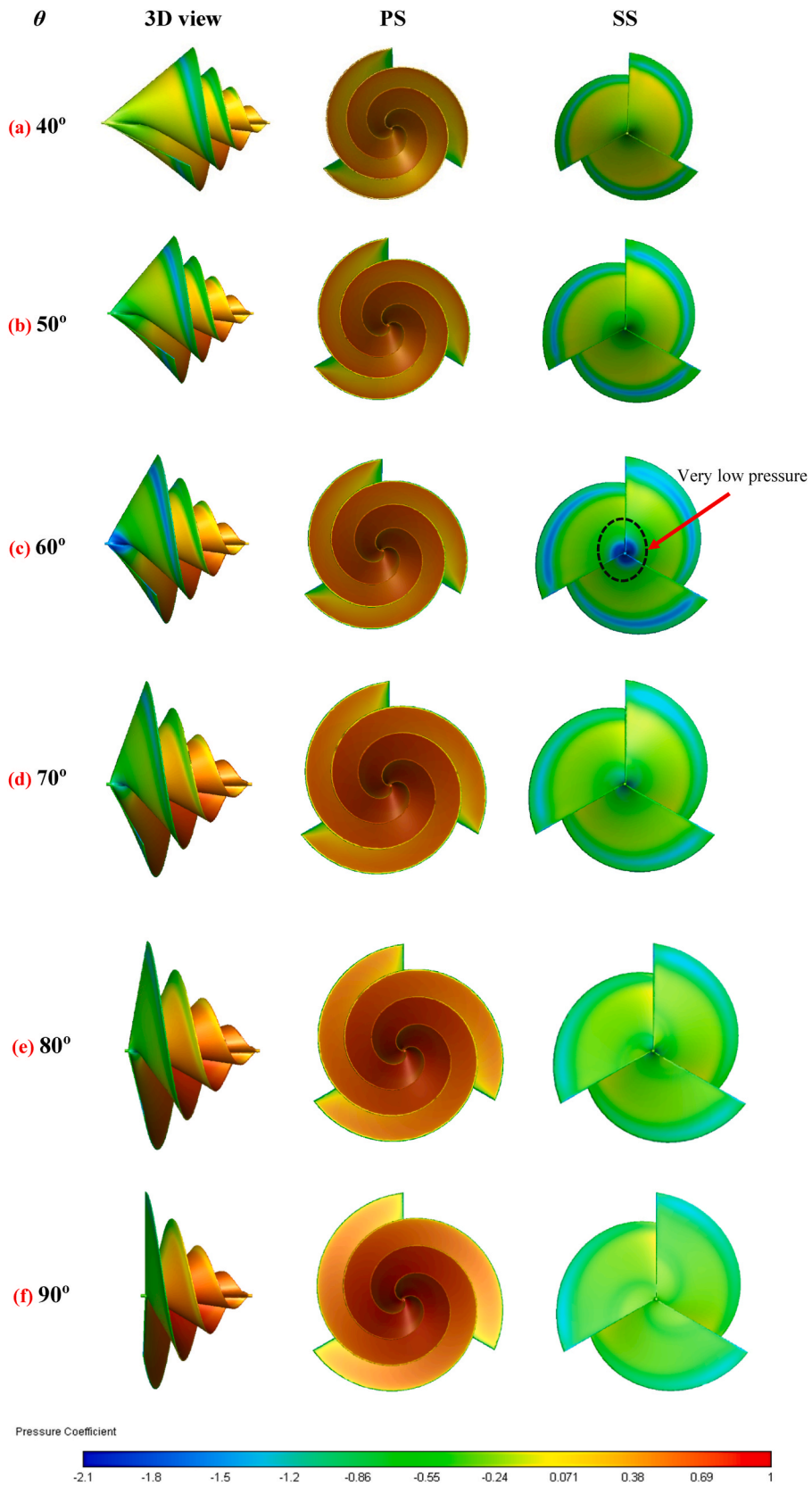
$C_{T \text{ Average}}$  of the conventional one. The maximum percentage increase in the  $C_{T \text{ Average}}$  is equal to 21% compared to the conventional turbine.

### 6. Conclusions

Small-scale wind turbines are employed where huge wind turbines cannot be constructed. This research gives essential information about the seashell-shaped wind turbine (spiral wind turbine SWT), a novel type of wind turbine built particularly for urban usage. Also, these turbines enjoy advantages over the rest of the types of wind turbines, whether vertical or horizontal axis, as the cut-in speed of this turbine is low, and it begins to rotate and produce power at a speed of about 2.5 m/s. Also, the noise generated by this turbine is low compared to others, which qualifies this turbine to work in urban areas. Also, this type of turbine does not need a means of control for guiding, as it is considered self-guiding and accepts wind flow from any direction.

In the presented study several configurations of the seashell turbine based on the spiral profile (logarithmic and Archimedean) have been investigated. The effect of the opening angle ( $\theta$ ) on the turbine performance was also examined for both types of spirals. For each spiral turbine, the opening angle ( $\theta$ ) was varied from 40° to 90° with a step of 10°. The equations of RANS are calculated employing an ANSYS-FLUENT solver to find the turbine torque coefficient ( $C_T$ ) and the turbine power coefficient ( $C_p$ ). The main findings from the presented examination proposed that the seashell-shaped wind turbine with the Archimedean spiral profile achieves better performance than the logarithmic profile. The results are concluded as follows.

1. It was found that the lowest value of the  $C_{T \text{ Average}}$  is about 0.05066 for the logarithmic spiral turbine with a  $\theta$  of 40°. While the highest  $C_{T \text{ Average}}$  of the logarithmic turbine is 0.1215 at a  $\theta$  of 90°.
2. The turbine of the Archimedes spiral profile with  $\theta$  of 40° obtains the highest  $C_{T \text{ Average}}$ , which is equal to 0.13993. While the turbine of the Archimedes spiral profile with a  $\theta$  of 90° has the lowest  $C_{T \text{ Average}}$ , which is 0.0654.
3. The value of the  $C_{T \text{ Average}}$  of the Archimedean spiral seashell turbine of 60° opening angle is at a high value, as it is approximately equal to 0.117.
4. The maximum value of the  $C_p$  of the logarithmic turbine is 0.20858 at a TSR of 1.75 for the turbine with  $\theta$  of 90°.
5. The maximum  $C_p$  of the Archimedean spiral turbine with  $\theta$  of 60° is more than the maximum  $C_p$  of all other configurations.
6. The turbine's peak power coefficient (max  $C_p$ ) was achieved at a TSR of 2.5 for the Archimedean spiral seashell turbine of  $\theta = 60^\circ$  and equals 0.2683.
7. Also, the Archimedean spiral seashell turbine of  $\theta = 60^\circ$  has the best operating range of all other configurations of the turbine.



(caption on next page)

Fig. 19. Pressure coefficient contours of a seashell-shaped wind turbine having an Archimedean spiral profile at different opening angles ( $\theta$ ) at  $\lambda$  of 2.

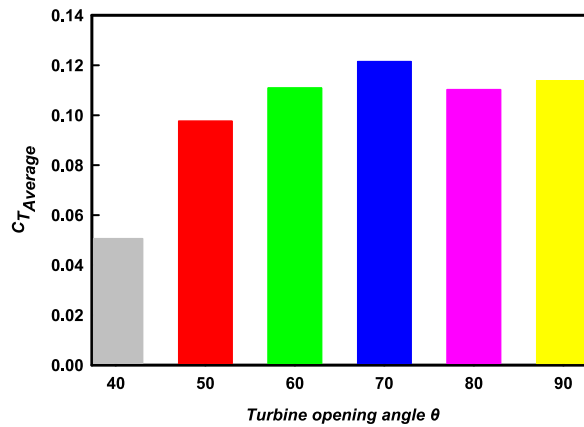


Fig. 20. Comparison of the average torque coefficient  $C_{T \text{ Average}}$  of a seashell-shaped wind turbine having a logarithmic spiral profile at different opening angles ( $\theta$ ).

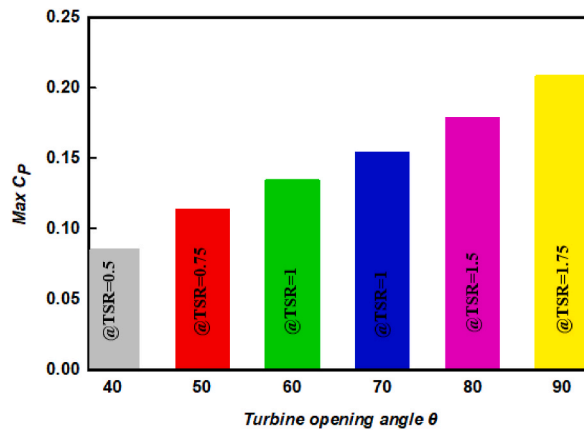


Fig. 21. Comparison of the max  $C_p$  of a seashell-shaped wind turbine having a logarithmic spiral profile at different opening angles ( $\theta$ ).

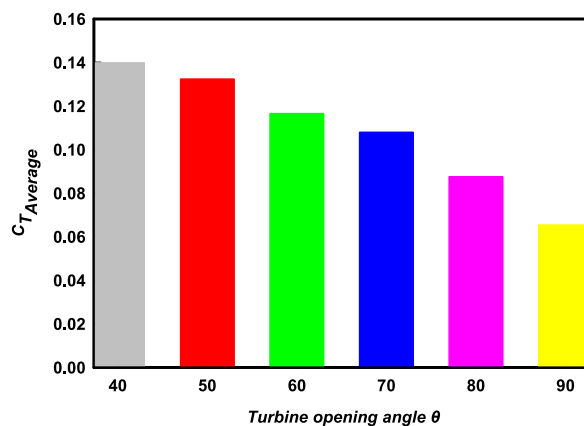


Fig. 22. Comparison of the average torque coefficient  $C_{T \text{ Average}}$  of a seashell-shaped wind turbine having an Archimedean spiral profile at different opening angles ( $\theta$ ).

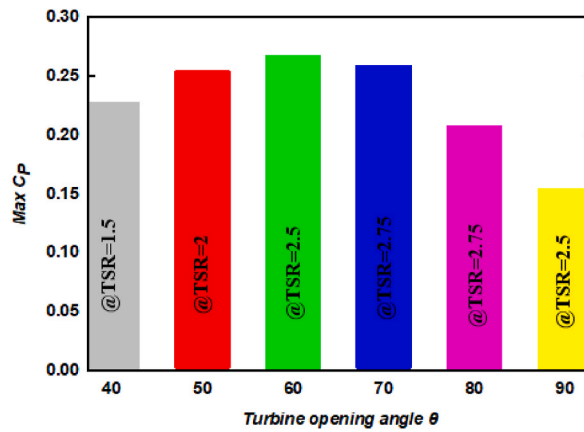


Fig. 23. Comparison of the max  $C_p$  of a seashell-shaped wind turbine having an Archimedean spiral profile at different opening angles ( $\theta$ ).

8. Additionally, the seashell-shaped wind turbine of the Archimedean spiral profile has a better performance than the conventional

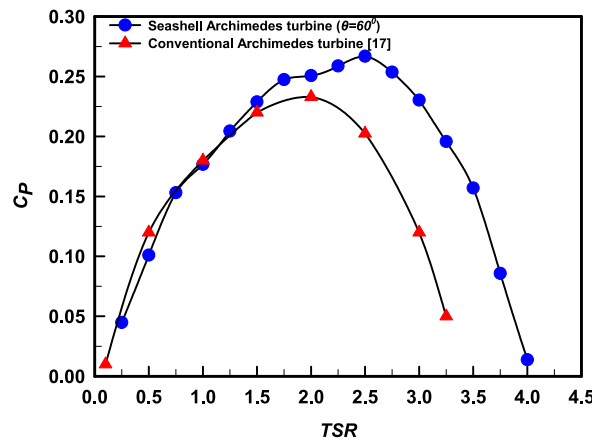


Fig. 24. Comparison of the power coefficient  $C_p$  of a seashell-shaped Archimedes wind turbine with a conventional Archimedes wind turbine [6].

Archimedean turbine studied previously.

- 9. The maximum  $C_p$  for the conventional Archimedean wind turbine equals 0.233, while for the seashell turbine of the Archimedean spiral profile the maximum  $C_p = 0.2683$ .
- 10. The maximum percentage increase in the  $C_p$  of the seashell-shaped wind turbine with the Archimedean spiral profile compared to the conventional Archimedes turbine equals 14.52%.

As for the important recommendations to be made in future studies, the aeroacoustics analysis of this new design was recommended for future studies. Also, it is recommended to study the effect of the casing on the performance of this new turbine.

**Author contribution statement**

Hossam Hamid: Conceived and designed the experiments; Performed the experiments; Contributed reagents, materials, analysis tools or data; Wrote the paper.

Rafea Mohamed Abd El Maksoud: Analyzed and interpreted the data.

**Data availability statement**

Data will be made available on request.

## Declaration of competing interest

The authors declare that they have no known competing financial interests or personal relationships that could have appeared to influence the work reported in this paper.

## Acknowledgments

Null.

## References

- [1] Peter Zhang, Stefan Gsanger, Small Wind World Report, 15-18 march, World Wind Energy Association, 2012.
- [2] A.P. Schaffarczyk, Introduction to Wind Turbine Aerodynamics, Springer publication, 2014.
- [3] Casini Marco, Small vertical axis wind turbines for energy efficiency of buildings, *J. Clean Energy Technol.* 4 (1) (2016).
- [4] Ho Song Ji, Joon Ho Baek, Rinus Mieremet, Kyung Chun Kim, The aerodynamic performance study on small wind turbine with 500 watt class through wind tunnel experiments, *Int. J. Reconfigurable Embed. Syst.* 1 (2016) 7–12.
- [5] K.C. Kim, H.S. Ji, Y.K. Kim, Q. Lu, J.H. Baek, R. Mieremet, Experimental and numerical study of the aerodynamic characteristics of an Archimedes spiral wind turbine blade, *Energies* 7 (12) (2014) 893–914.
- [6] S. Chaudhary, S. Jaiswal, R. Nanda, S. Patel, P. Kumar, Comparison of torque characteristics of Archimedes wind turbine evaluated by analytical and experimental study, *Int. J. Mechan. Product. Engin.* 4 (8) (2016) 75–78.
- [7] A.M. Labib, A.F. AbdelGawad, M.M. Nasseif, Effect of blade angle on aerodynamic performance of Archimedes spiral wind turbine, *J. Adv. Res. Fluid Mech. Thermal Sci.* 19 78 (1) (2021) 122–136.
- [8] W.A. Timmer, S. Toet, Verslag van de metingen aan de Archimedes in de large-snelheids wind tunnel vandnw, TU Delft, 2009.
- [9] S. Ebrahimi, M.A. Ghassemi, Numerical aerodynamics analysis of the Archimedes screw wind turbine, *Int. J. Multidiscip. Sci. Eng.* 12–15 (2018).
- [10] A. Safdari, K.C. Kim, Aerodynamic and structural evaluation of horizontal Archimedes spiral wind turbine, *J. Clean Energy Technol.* 3 (1) (2015) 34–38.
- [11] M. Ozeh, A. Mishra, X. Wang, Mini wind turbine for small scale power generation and storage (Archimedes wind turbine model), in: ASME 2018 International Mechanical Engineering Congress and Exposition, American Society of Mechanical Engineers Digital Collection, 2018.
- [12] H. Jang, D. Kim, Y. Hwang, I. Paek, S. Kim, J. Baek, Analysis of Archimedes spiral wind turbine performance by simulation and field test, *Energies* 12 (2019) 4624.
- [13] Y. Patil, Design, fabrication, and analysis of fibonacci spiral horizontal Axis wind turbine, *Int. J. Aerospace and Mechan. Engin.* 5 (1) (2018).
- [14] A.T. Mustafa, H.A. Jaleel, A comparison study between Archimedes spiral turbine and propeller turbine with wind attack angle effect, in: AIP Conference Proceedings, vol. 25, AIP Publishing LLC, 2020.
- [15] C. Ostia, J.M. Martinez, K.T. Coderes, G.J. Estacio, A.R. Ramchahi, J.V. Pulido, Development of a dual wind turbines using the Savonius and Archimedes spiral principle, in: 2018 IEEE 10th International Conference on Humanoid, Nanotechnology, Information Technology, Communication and Control, vols. 1–5, Environment and Management (HNICEM), 2018.
- [16] H.S. Ji, J.H. Baek, R. Mieremet, K.C. Kim, The aerodynamic performance study on small wind turbine with 500W class through wind tunnel experiments, *Int. J. Reconfigurable Embed. Syst.* 1 (2016) 7–12.
- [17] S.S. Rao, K. Shanmukesh, M.K. Naidu, P. Kalla, Design and analysis of Archimedes aero-foil wind turbine blade for light and moderate wind speeds, *Int. J. Recent Technol. Mechan. Electr. Engin.* 5 (8) (2018) 1–5.
- [18] U. Nepal, S. Sapkota, A. Bhattarai, H.P. Bashyal, Design, CFD Analysis and Modelling of Archimedean-Spiral Type Wind Turbine, IOE Graduate Conference, 2019.
- [19] M.A.A. Nawar, H.S.A. Hameed, A. Ramadan, Y.A. Attai, M.H. Mohamed, Experimental and numerical investigations of the blade design effect on Archimedes spiral wind turbine performance, *Energy* (2021), <https://doi.org/10.1016/j.energy.2021.120051>.
- [20] A.M. Labib, A.F. AbdelGawad, M.M. Nasseif, Effect of aspect ratio on aerodynamic performance of Archimedes, *The Egyptian Int. J. Engin. Sci. Technol.* 32 (2020) 66–72.
- [21] A.G. Refaie, H.S.A. Hameed, M.A.A. Nawar, Y.A. Attai, M.H. Mohamed, Qualitative and quantitative assessments of an Archimedes spiral wind turbine performance augmented by A concentrator, *Energy* 22 231 (2021), 121128.
- [22] F.R. Menter, Two-equation eddy-viscosity turbulence models for engineering applications, *AIAA J.* 32 (8) (1994) 1598–1605.
- [23] F. Porté-Agel, Y.T. Wu, H. Lu, R.J. Conzemius, Large-eddy simulation of atmospheric boundary layer flow through wind turbines and wind farms, *Wind Eng. Ind. Aerodyn* 99 (2011) 154–168.
- [24] D.C. Wilcox, Turbulence Modeling for CFD, vol. 93, DCW Industries, Inc., La Canada, California, 1993.
- [25] J. Franke, Introduction to the prediction of wind loads on buildings by computational wind engineering (CWE), in: T. Stathopoulos, C.C. Baniotopoulos (Eds.), *Wind Effects on Buildings and Design of Wind-Sensitive Structures*, Part of the CISM International Centre for Mechanical Sciences, vol. 493, 2007, pp. 67–103.
- [26] F.S. Lien, E. Yee, Y. Cheng, Simulation of mean flow and turbulence over a 2D building array using high-resolution CFD and a distributed drag force approach, *J. Wind Eng. Ind. Aerod.* 92 (2) (2004) 117–158.